

Inelastic Neutron and X-ray Scattering from Incommensurate Magnetic Systems

Peter Böni¹, Bertrand Roessli², Klaudia Hradil³

¹ *Physik Department E21, Technische Universität München, D-85748 Garching, Germany*

² *Laboratory for Neutron Scattering, Paul Scherrer Institut, CH-5232 Villigen PSI, Switzerland and*

³ *X-Ray Center, Vienna University of Technology A-1060 Vienna, Austria*

Neutrons and X-rays are powerful probes for studying magnetic and lattice excitations in strongly correlated materials over very wide ranges of momentum and energy transfers. In the focus of the present work are the incommensurate magnetic systems MnSi and Cr. Under application of a magnetic field, helically ordered MnSi transforms into a weak itinerant ferromagnet. Using polarized neutrons we demonstrate that the Stoner excitations are spin flip excitations. The amplitude (longitudinal) fluctuations associated with the magnon modes are already strong far away from T_C . Interestingly, even the non spin flip excitations associated with the Stoner modes are observable. In Cr, we have observed Kohn anomalies in the phonon spectrum at those incommensurate positions in reciprocal space, where the spin density wave is observed. The corresponding phonon and magnon modes are not coupled. In addition, an anomalous softening of a transverse phonon branch along the N-H zone boundary line is observed that is caused by strong electron phonon coupling. High resolution neutron scattering indicate that the low energy Fincher-Burke excitations may rather correspond to localized modes in momentum and energy and not to propagating collective modes. Finally, we demonstrate that in the near future it may become feasible to investigate excitations in very small samples thus allowing to measure the dynamics of strongly correlated materials under extreme conditions and in the vicinity of quantum phase transitions.

PACS numbers: 75.30.Ds, 63.20.Kr, 71.27.+a, 71.70.Gm

I. INTRODUCTION

Effects related to incommensurate magnetic or charge order have revealed many interesting effects in condensed matter physics. Recent examples include i) high- T_c superconductors, where antiferromagnetic fluctuations may be responsible for the pairing of the electrons¹, ii) multiferroic compounds such as the manganites RMnO_3 (R: lanthanide, alkaline metals)² or borates³, where a coupling between magnetic spiral-like order and the lattice or magneto-elastic coupling may lead to ferro-electric coupling, or iii) itinerant magnets such as MnSi, where a skyrmion lattice has recently been identified⁴. By measuring the collective excitations in these materials it is possible to determine the energy scales that are responsible for the competing interactions, which are the origin for the novel incommensurate orderings.

Two prototypical magnetic systems are in the focus of our present interest, namely MnSi and Cr. MnSi serves as a prototype system for a weak itinerant magnet exhibiting modulated magnetically ordered phases⁴ due to the competition between the Dzyaloshinskii Moriya and the exchange interaction^{5,6}. The incommensurate antiferromagnet Cr is brought into focus due to the fact that the excitation spectrum shows striking similarities with the magnetic excitations in high T_c -superconductors⁷. In order to access the important energy(E)-scales in these systems, various scattering techniques are to be used.

With the ongoing efforts to improve the E -resolution of inelastic X-ray beamlines approaching 1 meV, photons have become a valuable tool for investigating the lattice dynamics in solid state physics. In contrast to neutron scattering, the relative change of the energy of the pho-

tons during scattering is small, i.e. the scattering triangle remains essentially isosceles. Therefore, the phonon dispersions can be measured efficiently over large regions in momentum(\mathbf{Q})-space using area detectors. Compared to investigations with photons, the strengths of neutron scattering are a widely tunable E -resolution and the large interaction with the magnetic degrees of freedom. To take benefit of the individual probes, we have applied both techniques to investigate the dynamics in Cr and MnSi as described below.

II. MAGNETIC SCATTERING FROM ITINERANT FERROMAGNETS

First we describe inelastic neutron scattering experiments that were performed with polarized neutrons in MnSi, thus providing a direct means to observe single particle excitations in itinerant ferromagnets. According to the most simple model for ferromagnetism in delocalized systems, Stoner⁸ assumed that within a single band model the interaction between the spin up and spin down electrons leads to a separation of the bands by an exchange splitting Δ (Fig. 1(a)). The energy gain is partly compensated by an increase of the kinetic energy of the conduction electrons. In this picture, long range ferromagnetic order is destroyed by the thermal excitation of electrons between the spin split bands. Fig. 1(b) depicts the continuum of single particle excitations between the spin up and spin down bands and (c) shows the continuum of excitations within the bands. Also indicated in (b) is the spin wave branch of the collective excitations (magnons) that proceeds from $q = 0$ (Goldstone mode)

towards the Stoner continuum.

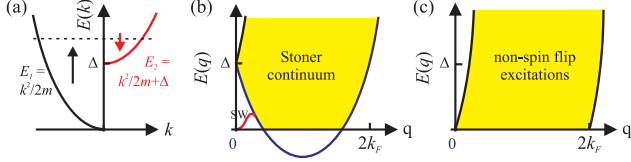


FIG. 1: The spin split bands are separated by the exchange splitting Δ as shown in (a). (b) shows the continuum of spin flip excitations between the two bands, i.e. the Stoner continuum. The spin wave (SW) branch extends from $q = 0$ towards the Stoner continuum. (c) shows the continuum of non spin flip excitations within a band.

Extensive measurements of the spin fluctuations in the ordered phase of MnSi using unpolarized neutrons have been performed by Ishikawa et al. many years ago⁹. These experiments were not sensitive to distinguish between spin flip and non spin flip contributions. In order to separate the contributions, we have investigated the magnetic excitation spectrum using inelastic neutron scattering with longitudinal polarization analysis.

Due to the lack of a symmetry center in the cubic crystal structure ($a_{\text{MnSi}} = 4.56 \text{ \AA}$) of MnSi (P2₁3), a left-handed magnetic spiral with a long period $\Lambda \simeq 185 \text{ \AA}$ is observed leading to magnetic satellite peaks close to the nuclear reflections (Fig. 2)¹⁰. Weak crystal electric fields pin the spirals along the $\langle 111 \rangle$ directions. Under application of a field $B \simeq 0.6 \text{ T}$ a ferromagnetic state is induced. Close to T_C and in a field $B \simeq 0.2 \text{ T}$, a skyrmion lattice develops that is stabilized by low energy fluctuations⁴. Apart from these modulated phases, the magnetic properties are considered to be those of a ferromagnet.

Fig. 3 shows contour maps of the spin flip (sf) and non spin flip (nsf) excitations of MnSi as measured in the field induced ferromagnetic state ($B = 0.7 \text{ T}$) at $T = 26 \text{ K}$ ($0.88 T_C$). The experiments were performed on the triple axis spectrometer IN20 at the Institut Laue-Langevin (ILL) around the (110) Bragg peak in a (110) plane using longitudinal polarization analysis (Fig. 2).

The sf-data in Fig. 3(a) clearly shows the spin wave branch emerging from the (110) Bragg peak becoming very steep near $\zeta = 0.8$. One can clearly distinguish two different regimes: i) at low E -transfer $E < 2.5 \text{ meV}$ ($0.9 < \zeta < 1.0$) a ferromagnetic spin wave dispersion is observed given by $E_q = Dq^2$ with $D = 23.5 \pm 3.0 \text{ meV \AA}^2$ ¹¹ and ii) at large E -transfers the excitations can be directly identified in terms of Stoner excitations as depicted in Fig. 1(b). A close inspection of the data shows that only the spin waves renormalize with increasing T , while the Stoner excitations do not change significantly¹².

The nsf-data (Fig. 3(b)) shows at low energy transfers large cross sections. They are identified as longitudinal magnetic fluctuations, which have also been observed in Ni¹³ and EuS¹⁴. However, due to the strong

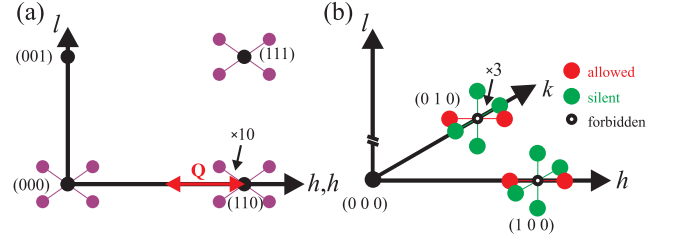


FIG. 2: (a) Reciprocal lattice of helimagnetic MnSi showing the position of the magnetic satellites close to the nuclear Bragg reflections. (b) depicts the reciprocal lattice of Cr when it is prepared in a single \mathbf{Q} state with \mathbf{Q} parallel to the $[100]$ -direction. Therefore, magnetic satellites that are allowed by symmetry along the $[010]$ and $[001]$ directions are silent. The incommensurabilities are exaggerated by factors of 10 and 3 for MnSi and Cr, respectively.

electronic correlations in MnSi leading to a large magnetic correlation length, the longitudinal modes are already strong much further away from T_C namely already at $0.88 T_C$, where the present measurements have been conducted. These modes diverge near T_C due to the increasing magnon-magnon interactions¹⁵. The longitudinal modes extend into the regime of single particle excitations. The distribution of their spectral weight looks qualitatively similar as the simple model shown in Fig. 1(c).

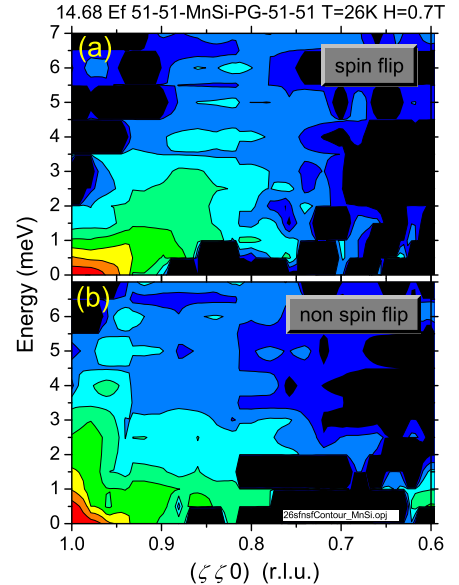


FIG. 3: Contour maps of MnSi measured along the $[110]$ direction at $T = 26 \text{ K}$ and in a field $B = 0.7 \text{ T}$. The sf data (a) clearly indicates the spin wave branch merging into the Stoner continuum. The contours of the nsf scattering (b) show the steep longitudinal phonon branch as well as the longitudinal fluctuations, which extend to high energy transfers.

To obtain a more quantitative interpretation of the

data we show in Fig. 4 cuts through the contours of Fig. 3 at $E = 5$ meV. The Stoner excitation in the spin flip channel is clearly visible near $\zeta = 0.83$. The nsf scattering is very weak. The data sets were fitted using a double Lorentzian scattering function

$$S(q, E) = \frac{q_d^2}{\kappa_1^2 + q^2} \frac{1}{2\pi} \frac{E\Gamma}{(E - E_q)^2 + \Gamma^2} \langle n + 1 \rangle \quad (1)$$

convoluted with the resolution function, where Γ is the linewidth parameterized by $\Gamma = Aq^{2.5}$ and κ_1 is the inverse correlation length¹⁶. The Lorentzian is centered at the spin wave energy $E_q = Dq^2$, where D is the stiffness. In the case of quasielastic scattering, $D = 0$ and κ_1 assumes a finite value¹⁴. $\langle n + 1 \rangle$ is the thermal population factor. The fit of the sf-data demonstrates that the parameter $D_{sf} = 35$ meVÅ² for the Stoner excitations is indeed significantly larger than the stiffness parameter of the spin wave mode at low E -transfers, $D_{sw} = 23.5$ meV¹¹. In contrast, the best fits to the nsf-data converge towards the parameters $D_{nsf} = 0$ and $A_{nsf} = 44$ meVÅ^{2.5}. A_{nsf} is about twice as large as the parameter $A = 19.6$ meVÅ^{2.5} measured in the paramagnetic phase of MnSi at small momentum and E -transfer¹⁶. This large A_{nsf} is in line with the increased stiffness of the Stoner excitations. A forced fit to the data fixing D_{nsf} at 23.5 meV leads to an increased χ^2 (broken line in Fig. 4). It does not represent the data well.

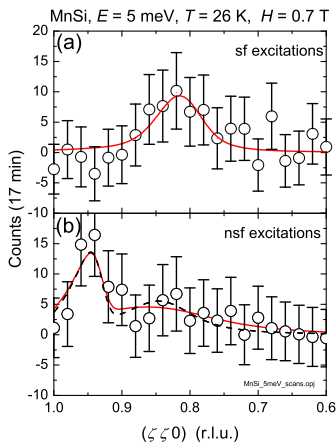


FIG. 4: Constant energy scans for $E = 5$ meV at $T = 26$ K and $B = 0.7$ T. (a) shows a Stoner excitation near $(0.8, 0.8, 0)$. The solid line is a fit to equation (1). (b) The magnetic nsf scattering is barely visible. The solid and the broken lines are fits to equation (1) assuming a diffusive or a propagating mode, respectively, and a cross section for the acoustic phonon at $\zeta = 0.95$.

We point out that the measurements shown here have been conducted at very large $|\mathbf{q}| \gg 2\pi/\Lambda$, where the helical correlations are expected to be of no relevance. Indeed, the contour plot for $E = 0$ (Fig. 5) demonstrates

that the magnetic satellites are very close to the nuclear zone centre.

Driven by the discovery of a non-Fermi liquid state under high pressure and a skyrmion lattice for $B = 0.2$ T, the magnon spectrum in the helical phase has recently been investigated with high resolution triple axis spectroscopy using cold neutrons. Around the magnetic satellites, a rich spectrum of spin excitations are observed that are identified as helimagnons¹⁷. Using a model¹⁸ based on only three parameters, namely the pitch of the helix, the spin wave stiffness, and an overall amplitude of the signal one can account for all spectra, demonstrating that helimagnons are a universal characteristics of systems with weak chiral interactions.

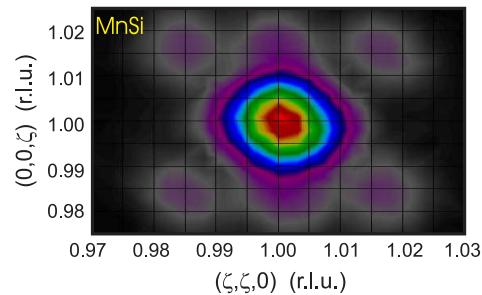


FIG. 5: Elastic neutron scattering around the $(1\ 1\ 0)$ Bragg peak showing the magnetic satellite peaks along the $\langle 111 \rangle$ directions. The weak spots at $(1, 1, 0.985)$ and $(1, 1, 1.015)$ are the result of the out of plane satellites, which become visible due to the coarse vertical resolution.

In conclusion, we have shown that inelastic neutron scattering with polarized neutrons allows to study the single particle excitations in weak itinerant magnets. The results prove directly that the Stoner excitations are spin flip excitations. Unexpectedly, the nsf fluctuations show significant cross sections even at high energy transfers. To disentangle the complicated spectra and to determine the helicity of the helimagnons it would be of great value to extend the polarized beam measurements to small momentum transfers using high resolution spectroscopy. Indeed, recently it was shown that the paramagnetic¹⁹ and helimagnetic²⁰ excitations in MnSi have a chiral contribution, which is large even close to T_C .

III. MAGNON AND PHONON EXCITATIONS IN ANTIFERROMAGNETIC CR

In metals with Fermi surfaces, nesting enhances the number of transitions at the nesting wavevectors \mathbf{Q}_n when compared to other wavevectors. The nesting greatly increases the number of possible electronic transitions at \mathbf{Q}_n , which may lead to the formation of spin density waves (SDW)^{21,22} and/or may soften and broaden phonons²³. Both effects are observed in strongly correlated electron systems, i.e. in the copper oxide superconductors^{24,26} and in elemental Cr²⁵. Both ma-

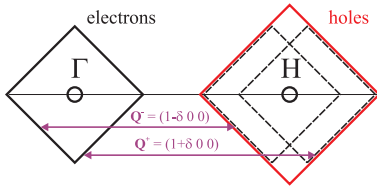


FIG. 6: Schematic cross section of the Fermi surface in the (1 1 0) plane of Cr. Nesting vectors \mathbf{Q} connect the electron with the hole surface.

terials show a long history of intensive investigations.

In contrast to MnSi, where the magnetic ordering is caused by the non-centrosymmetric crystal structure leading to a pronounced Dzyaloshinskii-Moriya (DM) interaction^{5,6}, the incommensurate magnetic ordering in Cr is the result of the nesting properties of the electron and hole Fermi surface²² as explained in Fig. 6. Despite numerous investigations, the magnetic excitations in Cr are still not well understood and some of the controversial experimental results concerning the Fincher-Burke (FB) modes²⁷ have only recently been reinvestigated²⁸.

Cr crystallizes in a simple body centered cubic structure with a lattice constant $a_{Cr} = 2.88 \text{ \AA}$. It undergoes a transition from the paramagnetic phase to a SDW phase at $T_N = 311 \text{ K}$ characterized by propagation vectors $\mathbf{Q}^\pm = (1 \pm \delta, 0, 0)$ with $\delta = 0.048$. The corresponding magnetic satellite peaks are visible near the forbidden Bragg reflections of the bcc structure, i.e. $h+k+l = \text{odd}$ (Fig. 2). In the transverse spin-density wave (TSDW) phase $T_{sf} < T < T_N$ the magnetic moments are aligned perpendicular to \mathbf{Q}^\pm . At $T_{sf} = 121 \text{ K}$ the magnetic structure undergoes a first order phase transition to a longitudinal spin-density wave (LSDW) phase with the spins aligned along \mathbf{Q}^\pm .

Due to the SDW, there is a distortion of the lattice with twice δ . Indeed, charge density waves (CDW) were observed using both neutron and X-ray diffraction^{30,31}. Recently even pressure measurements were performed³². The CDW can be induced either by Fermi surface nesting or by a strain wave induced by magnetoelastic coupling to the SDW.

As explained above, the interaction of the conduction electrons with the lattice vibrations enhanced by anomalies of the Fermi surface leads to anomalous phonon dispersions. Using inelastic neutron scattering, four regions have been identified where transverse acoustic phonons show anomalous behavior that can be traced back to nesting³³. The two most pronounced anomalies occur near the N- and H-point as shown in Fig. 7. Because of the appearance of a SDW near H, this point is of particular interest. However, because of the coarse \mathbf{Q} -resolution of neutron scattering the phonon anomaly may be washed out. Here, the improved \mathbf{Q} -resolution of synchrotron radiation may help to highlight if there is a correspondence between the phonon anomalies and Fermi surface nesting in Cr near H.

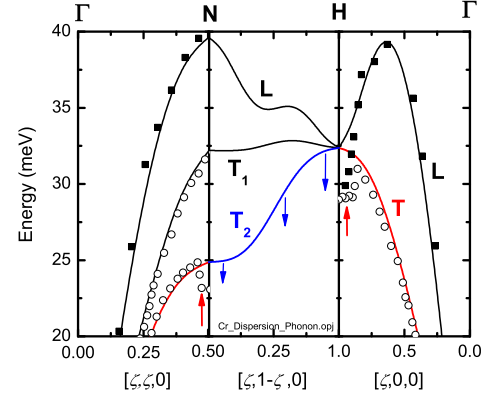


FIG. 7: Comparison of the phonon dispersion as calculated by means of the Born-von-Kármán model along the high symmetry directions $[\zeta \zeta 0]$ and $[\zeta 0 0]$. The data points from reference³³ show strong anomalies near the N and H points as indicated by red arrows. Our results show that the T2 branch along the whole zone boundary line N-H softens as indicated by three blue arrows.

A. Magnetic excitations in Cr

In order to obtain an overview on the spectral distribution of the magnetic excitations in Cr we show in Fig. 8 a contour plot of the inelastic intensity in the TSDW-phase at 136 K that was measured with high energy and momentum resolution using cold neutrons ($E_f = 5.64 \text{ meV}$). Most dominant are the very steep excitations that emerge from the incommensurate positions. Because of the very large velocity of the excitations, $c \simeq 1500 \text{ meV \AA}$, the dispersion branches cannot be resolved^{34,35}. Taking into account that various simple band models predict a velocity $c \simeq v_F/\sqrt{3}$ where v_F is the Fermi velocity³⁶, this high c value seems reasonable. At high energy transfers, $E > 30 \text{ meV}$ the dispersion branches bend towards the commensurate position³⁴ because of the increasing spectral weight of the phason modes with increasing energy^{7,37}.

Other important features are the low-energy excitations at $E < 10 \text{ meV}$, which occur only in the TSDW phase^{28,29}. Clearly visible are the modes at $E \simeq 4.5 \text{ meV}$ and at 8 meV (Fig. 9) as already observed by Fincher et al. demonstrating the correspondence of our data with the previous data³⁴. In addition, two modes at $\simeq 1.016 \text{ \AA}^{-1}/\simeq 3.8 \text{ meV}$ and $\simeq 0.984 \text{ \AA}^{-1}/\simeq 6.8 \text{ meV}$ are visible, which have no counter parts at the symmetry related positions $\simeq 0.984 \text{ \AA}^{-1}$ and $\simeq 1.016 \text{ \AA}^{-1}$, respectively. The comparison with previous data measured with lower resolution^{27,29} raises the question if dispersing modes alone can explain the data or if local modes have to be included.

Moreover, it is not easily understandable why the mea-

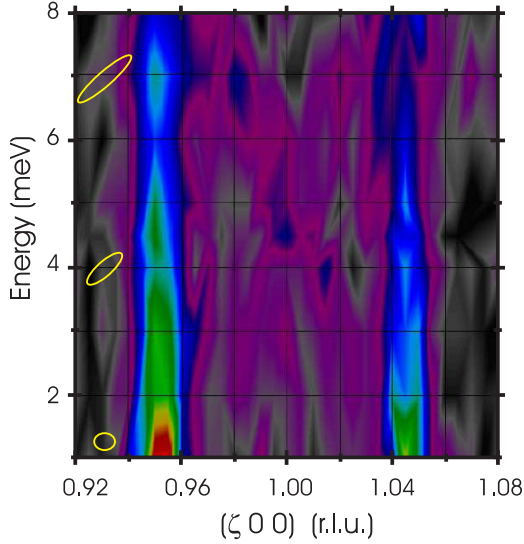


FIG. 8: Contour map of the excitation spectrum as measured in the transverse spin density wave phase of Cr at $T = 136$ K. The intense peak near 4.5 meV and $\mathbf{Q} = (1, 0, 0)$ is the Fincher mode. Note the additional peak near $(1.02, 0, 0)$ and 3 meV that has no counter part at $(0.98, 0, 0)$. The ellipsoids indicate the resolution of the triple axis spectrometer TASP³⁸ for various E -transfers.

sured modes have very similar intensities although the thermal population factor $\langle n+1 \rangle$ would predict a significantly higher intensity for the 3.8 meV mode when compared with the 6.8 meV mode, provided that both modes belong to the same dispersion as alluded to in Ref.²⁷. We may speculate that mode-coupling has to be involved. To answer these questions, more precise measurements with better statistics have to be performed.

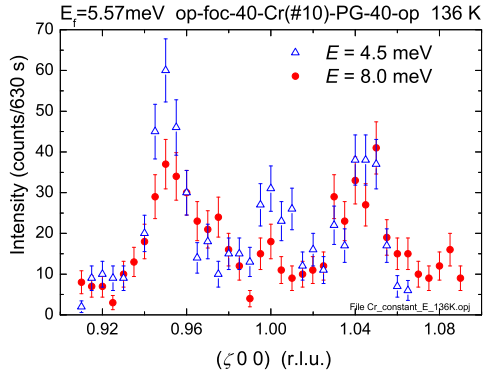


FIG. 9: Constant- E scans showing the Fincher mode at $(1, 0, 0)$ for $E = 4.5$ meV and a weak mode at 8 meV that was already observed in Ref.³⁴.

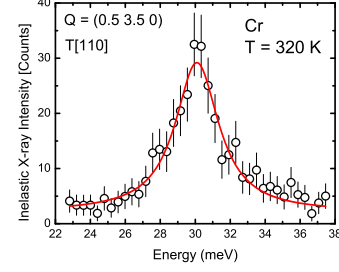


FIG. 10: Raw data from inelastic X-ray scattering as function of energy transfer at $T = 320$ K and $\mathbf{Q} = (0.5, 3.5, 0)$. The solid line corresponds to a fit assuming a Lorentzian.

B. Phonon softening in Cr

The goal of the experiments using synchrotron radiation was to determine the precise \mathbf{q} -position of the anomalous softening of the phonons and to compare it with the nesting features of the Fermi surface of Cr. In order to improve in \mathbf{Q} -resolution over the previous experiments using inelastic neutron scattering³³, we applied inelastic X-ray scattering. The experiment was performed at beam line ID-28 at ESRF using a Cr single crystal with the dimensions $2 \times 2 \times 2$ mm³. The phonon dispersion was investigated near the H-point and the measurements extended along the zone boundary to the N-point³⁹. In addition to previous measurements, the phonon dispersion along the line connecting the H-point and the N-point (Fig. 7) was explored for the first time.

Fig. 10 shows a phonon at $\mathbf{Q} = (0.5, 3.5, 0)$ that belongs to the acoustic $[1\ 1\ 0]$ T2 branch. Obviously, the position of the phonons can be measured with high precision. The solid line is a fit assuming a Lorentzian. Following this result, the dispersion of the phonons was determined in detail for \mathbf{Q} along $[1\ 0\ 0]$ as well as along the N-H line³⁹.

The measured dispersions near $(\frac{1}{2}\ \frac{1}{2}\ 0)$ and $(1\ 0\ 0)$ are shown in Fig. 11 (circles) and compared with the theoretical prediction based on a simple Born-von-Karman model (triangles). Along the $[1\ 1\ 0]$ direction, the maximum softening is observed exactly at the zone boundary N. In contrast, the H-phonon softens at the incommensurate position $\delta = 0.05$ where the SDW satellites occur and not at the zone boundary $(1\ 0\ 0)$ as reported previously (Fig. 7)³³.

Similar measurements have been conducted at various \mathbf{Q} -positions across the zone boundary line N-H. Fig. 12 summarizes the softening of the measured phonons when compared with a Born-von-Kármán model along the $[1\ 0\ 0]$ direction (circles) and along the zone boundary N-H (triangles). In the $[1\ 0\ 0]$ direction, the phonon softening has a distinct minimum at the nesting wavevector $\mathbf{Q}^\pm = (0.95, 0, 0)$. Surprisingly, a strong anomaly also appears along the entire zone boundary line N-H indicating that strong electron phonon coupling limited to a small range

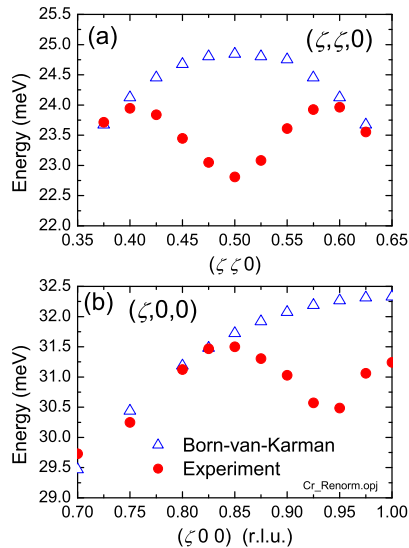


FIG. 11: (a) and (b) show the dispersion of the phonons near the N and H-points, respectively. The phonons along $[\zeta\zeta0]$ soften directly at the N-point while the phonons along $[\zeta00]$ soften at the nesting position, where the SDW ordering is observed (Fig. 8).

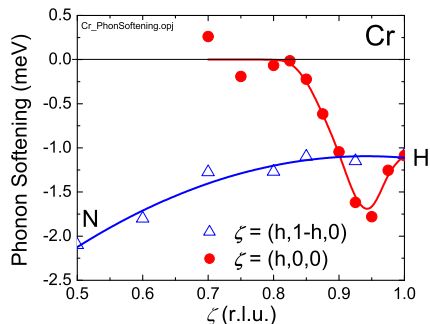


FIG. 12: Difference $E_{BvK} - E_{exp}$ between the Born-von-Kármán and the experimental phonon dispersions along the zone boundary N-H (triangles) and along the high symmetry direction Γ -H (circles).

of wavevectors can also result in strong phonon anomalies without invoking nesting. This observation implies that the phonon anomalies in copper oxide superconductors may also be explained by an enhanced electron-phonon coupling without invoking novel collective modes or some hidden nesting of the Fermi surface³⁹.

Additional measurements in the paramagnetic phase of Cr show a similar softening of the phonons close to the zone boundaries discussed above. In particular, the strong softening at $\mathbf{Q}^\pm = (0.95, 0, 0)$ persists demonstrating that the magneto-elastic coupling is small. Therefore, the nesting of the Fermi surface is responsible for the

Kohn anomaly in the phonon spectrum and the SDW below $T_N = 311$ K at \mathbf{Q}^\pm . They evolve independently with temperature.

In conclusion, we have shown that the incommensurate magnetic excitations in Cr can be interpreted in terms of electron hole excitations at the Fermi surface. Strong electron-phonon coupling without invoking nesting leads to a pronounced softening of the T2 phonon branch along N-H, i.e. away from \mathbf{Q}^\pm . We have provided evidence that the low energy excitations in the TSDW phase may not be explained in terms of a mode having a dispersion as proposed in Ref.²⁷.

IV. SMALL SAMPLES - EXTREME CONDITIONS

Studying quantum phase transitions by applying pressure, magnetic fields or by doping has proven to be a successful route to identify materials with novel properties. In MnSi, the application of pressure leads to the suppression of helical order near $p_c = 1.46$ GPa accompanied by the appearance of a partially ordered magnetic state and a non Fermi liquid phase⁴⁰. In Cr, antiferromagnetic order is suppressed around $p = 10$ GPa³². Neutron scattering as well as X-ray synchrotron scattering have provided valuable information about the vanishing of the order parameters, however, the present day sensitivity of neutron spectrometers is not sufficient to also characterize the spectrum of the magnetic and lattice excitations close to the quantum phase transitions because the samples are usually very small⁴¹.

Measurements of phonon dispersions may be conducted using inelastic X-ray scattering because only small samples are necessary and the \mathbf{Q} - and E -resolutions are often sufficient as shown in section IIIB. Inelastic magnetic scattering by X-rays is so far impossible because the magnetic cross sections are very small. In the following we demonstrate the feasibility of inelastic neutron scattering on small samples using supermirror focusing guides⁴², to generate very small but intense neutron beams at the sample position of the thermal triple axis instrument PUMA at FRM II.

To perform the experiment, a focusing guide with a length of 500 mm as described in Ref.⁴³ has been installed between the monochromator and the sample position. In the first instance we used a neutron CCD camera to both correctly align the guide and to analyze the shape and intensity of the beam at the sample position. These measurements show that the beam has a FWHM of approximately 2 mm in the horizontal direction and 8 mm in the vertical direction at the sample position. Such a beam size is ideal for studying samples with mm dimensions, unlike the conventional PUMA profile where the primary beam has dimensions of roughly 25 mm in the horizontal direction and 28 mm in the vertical direction and any adjustment for sample size is done by adjustable, neutron absorbing slits. The CCD camera images also revealed

that using the guide results in a very low background.

We have performed successful test experiments on two different samples. Firstly, a small single crystal of Cr with dimensions $2 \times 2 \times 2 \text{ mm}^3$ was investigated. Samples of this size can typically be used in a Paris-Edinburgh high pressure cell. Using the focusing guide, we were able to observe amongst other things the change in intensity of the magnetic excitations in the TSDW phase with increasing temperature (Fig. 13). Note that the counting time per point of 10 min corresponds to the typical counting time (13 min) used to collect the data in Fig. 3 of Ref.³⁴. Clearly, because of the coarse \mathbf{Q} -resolution due to the focusing, the fine structure of the spectrum is wiped out. Still, for the determination of the energy scale of the excitations versus pressure, inelastic measurements are feasible.

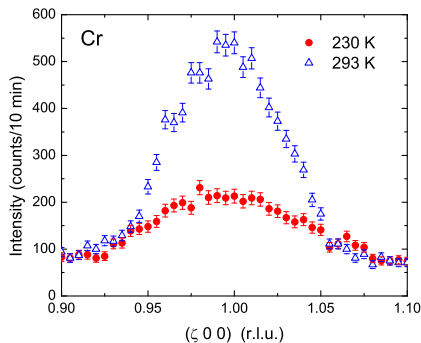


FIG. 13: Temperature dependence of the magnetic excitations in Cr as measured at $T = 230 \text{ K}$ and 293 K around the $(1\ 0\ 0)$ Bragg reflection at an energy of 4 meV .

In a second experiment we measured phonons in two different samples of quartz (SiO_2). The small and the large samples have a volume of 8 mm^3 and 2000 mm^3 , respectively (Fig. 14). The comparison allows a direct calibration between the conventional PUMA configuration and the configuration with a focusing guide. The results show that it is indeed possible to measure the acoustic transverse phonon at $(-0.9, 2.0, 0)$ with high precision within a reasonable time. Actually the comparison of the two measurements demonstrates that the results with the focusing guide provide a much cleaner spectrum and a lower background. Of course, the performance can be further increased without a significant loss in intensity if a second focusing guide is used between the sample and the analyzer⁴¹ and if the critical angle of reflection of the focusing guide is increased from $m = 3$ to $m = 7$ ⁴⁴.

Concluding, we have shown that advanced neutron optics allows the investigation of magnons and phonons under extreme conditions using small crystals providing a good E - and \mathbf{Q} -resolution. Focusing techniques for inelastic neutron scattering facilitate the exploration of new areas of science, where traditional experiments have been restricted due to the requirement of large samples.

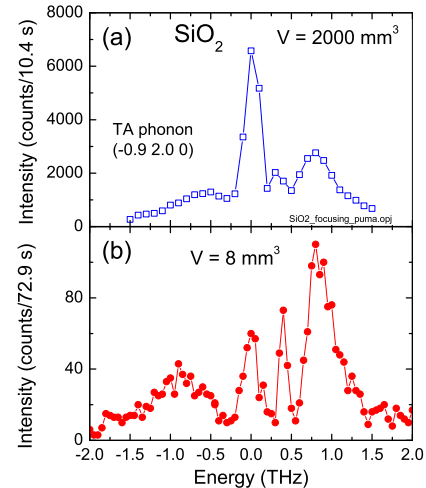


FIG. 14: Measurements of a transverse acoustic phonon in quartz. (a) Normal PUMA configuration using a doubly focusing monochromator. (b) Same measurement using a flat monochromator combined with a focusing guide. The small sample is 250 times smaller than the big sample.

V. CONCLUSIONS

Experiments using polarized neutrons allow the separation of phonon modes from magnon modes and furthermore between transverse and longitudinal fluctuations in magnetic systems. In MnSi it is observed that the Stoner excitations can be clearly identified in terms of spin flip excitations of the conduction electrons. The non spin flip scattering provides direct information on the amplitude fluctuations in the single particle regime. In addition, we found evidence that the low energy excitations in Cr (Fincher-Burke modes) may not be explained solely by assuming modes with a dispersion. Surprisingly the modes are asymmetric with respect to the $(1\ 0\ 0)$ position²⁹. The combination of inelastic X-ray and neutron scattering indicates that the Kohn anomaly near the H-point occurs at the same position as the spin density wave demonstrating that both effects are caused independently by the nesting properties of the Fermi surface of Cr. As a new feature, the X-ray results imply that the phonons are softened along the whole zone boundary line N-H due to electron-phonon interactions.

We have shown that the inelastic scattering of neutrons and X-rays provide complementary information on the lattice dynamics and the spectrum of the magnetic excitations in strongly correlated materials. While neutron scattering provides high-energy resolution and moderate \mathbf{Q} -resolution, X-rays provide sufficient \mathbf{Q} -resolution thus allowing to map out the softening of phonons near the zone boundaries of transition metals like Cr.

Finally we have evaluated the possibilities of performing inelastic neutron scattering from small samples us-

ing advanced focusing techniques. By means of focusing guides the intensity of neutron beams at the sample position can be increased rather dramatically thus allowing the investigation of sample with a volume of a few mm³⁴⁵. Therefore, samples under extreme conditions can be investigated near quantum phase transitions. With the advancement of next generation neutron sources using halo isomers that provide polarized neutron beams of very high brilliance⁴⁶, neutron scattering may make a big leap towards the investigation of excitations in samples that are much smaller than 1 mm³.

ACKNOWLEDGMENTS

We thank S. Dunsiger, M. Janoschek, D. Lamago, R. Mole, S. Mühlbauer, P. Niklowitz, C. Pfeiderer, D.

Reznik, and C. Schanzer for very useful discussions and assistance during the course of the experiments. This work is based on experiments performed at the FRM II in Garching, the Swiss Spallation Source SINQ, the HFR at the Institut Laue-Langevin, and the ESRF in Grenoble. We gratefully acknowledge financial support from the research unit on Quantum Phase Transitions FOR960 of the German Science Foundation (DFG). Part of the work was supported by the Swiss National Science Foundation through MaNEP and by the project 226507-NMI3 within the seventh framework program FP7 of the EU.

-
- ¹ Tranquada J et al. 2004 Nature **429** 534
 - ² Tokura Y 2003 Phys. Today **56** 50
 - ³ Janoschek M, Fischer P, Schefer J, Roessli B, Pomjakushin V, Meven M, Petricek V, Petrakovskii G, Bezmaternikh L (2010) Phys. Rev. B **81** 094429
 - ⁴ Mühlbauer S, Binz B, Jonietz F, Pfeiderer C, Rosch A, Neubauer A, Georgii R, Böni P 2009 Science **323** 915
 - ⁵ Dzyaloshinskii L 1958 J. Phys. Chem. Solids **4** 241
 - ⁶ Moriya T 1960 Phys. Rev. **120** 91
 - ⁷ Endoh Y, Böni P 2006 J. Phys. Soc. Jpn. **75** 111002
 - ⁸ Stoner E 1938 Proc. Roy. Soc. A **165** 372
 - ⁹ Ishikawa Y, Shirane G, Tarvin J A, Kohgi M (1977) Phys. Rev. B **16** 4956
 - ¹⁰ Tanaka M, Takayoshi H, Ishida M, Endoh Y (1985) J. Phys. Soc. Jpn. **54** 3232
 - ¹¹ Tixier S, Böni P, Endoh Y, Roessli B, Shirane G 1999 Physica B **241-243** 613
 - ¹² Semadeni F, Böni P, Endoh Y, Roessli B, Shirane G 1999 Physica B **267-268** 248
 - ¹³ Böni P, Martínez J L, Tranquada J M (1991) Phys. Rev. B **43** 575
 - ¹⁴ Böni P, Roessli B, Görlitz D, Kötzler J, Phys. Rev. B **65** 144434
 - ¹⁵ Villain J (1970) Solid State Commun. **8** 31
 - ¹⁶ Ishikawa Y, Noda Y, Uemura Y J, Majkrzak C F, Shirane G (1985) **31** 5884
 - ¹⁷ Janoschek M, Bernlochner F, Dunsiger S, Pfeiderer C, Böni P, Roessli B, Link P, Rosch A (2010) Phys. Rev. B **81** 214436
 - ¹⁸ Belitz D, Kirkpatrick T R, Rosch A (2006) Phys. Rev. B **73** 054431
 - ¹⁹ Roessli B, Böni P, Fischer W, Endoh Y 2002 Phys. Rev. Lett. **88** 237204
 - ²⁰ Roessli B, Böni P, Fischer W E, Endoh Y (2004) Physica B **345** 124
 - ²¹ Overhauser A W, Arrott A 1960 Phys. Rev. Lett. **4** 226
 - ²² Overhauser A W 1962 Phys. Rev. **128** 1437
 - ²³ Kohn W 1959 Phys. Rev. Lett. **2** 393
 - ²⁴ Djajaputra D and Ruvalds J 1999 Solid State Commun. **111** 199
 - ²⁵ Fawcett E (1988) Rev. Mod. Phys. **60** 209
 - ²⁶ Reznik D 2010 Advances in Condensed Matter Physics **2010** 523549
 - ²⁷ Burke S K, Stirling W G, Ziebeck K R A, Booth, J G 1983 Phys. Rev. Lett. **51** 494
 - ²⁸ Hiraka H, Endoh Y, Böni P, Fujita M, Yamada K, Shirane G 2003 Phys. Rev. B **67** 064423
 - ²⁹ Hiraka H, Böni P, Yamada K, Park S, Lee S-H, Shirane G 2004 Phys. Rev. B **70** 144413
 - ³⁰ Pynn R, Press W, Shapiro M S, Werner S A 1976 Phys. Rev. B **13** 295
 - ³¹ Tsunoda Y, Mori M, Kunitomi N, Teraoka Y, Kanamori J 1974 Solid. State Commun. **14** 287
 - ³² Jaramillo R, Feng Y, Lang J C, Islam Z, Srajer G, Littlewood P B, Whan D B, Rosenbaum T F 2009 Nature **459** 405
 - ³³ Shaw W M, Muhlestein L D 1971 Phys. Rev. B **4** 969
 - ³⁴ Fincher C R, Shirane G, Werner S A 1981 Phys. Rev. B **24** 1312
 - ³⁵ Böni P, Sternlieb B, Shirane G, Roessli B, Lorenzo J E, Werner S A 1998 Phys. Rev. B **57** 1057
 - ³⁶ Fedders P A, Martin P C (1966) Phys. Rev. **143** 245
 - ³⁷ Fishman R S, Liu S H 1996 Phys. Rev. B **54** 7252
 - ³⁸ Semadeni F, Roessli B, Böni P (2001) Physica B **297** 152
 - ³⁹ Lamago D, Hoesch M, Krisch M, Heid R, Bohnen K-P, Böni P, and Reznik D (2010) Phys. Rev. B **82** 195121
 - ⁴⁰ Pfeiderer C, Reznik D, Pintschovius L, v. Löhneysen H, Garst M, Rosch A (2004) Nature **427** 227
 - ⁴¹ Niklowitz P G, Pfeiderer C, Mühlbauer S, Böni P, Keller T, Link P, Wilson J A, Vojta M, Mydosh J A (2009) Physica B **404**, 2955
 - ⁴² Böni P (2008) Nucl. Instrum. Methods A **586** 1-8
 - ⁴³ Mühlbauer S, Stadlbauer M, Böni P, Schanzer C, Stahn J, Filges U (2006) Physica B **385-386** 1247 (2006)
 - ⁴⁴ <http://www.swissneutronics.ch/products/coatings.html>
 - ⁴⁵ Hils T, Böni P, Stahn J (2004) Physica B **350** 166
 - ⁴⁶ Habs D, Gross M, Thierolf P G, Böni P (2011) Appl. Phys. B., DOI10.1007/s00340-010-4276-3 (accepted for publication)